

# A Bio-inspired Hexapod Robot with Noncircular Gear Transmission System

Ke-Jung Huang, Shen-Chiang Chen, Meng-Ching Tsai, Fnag-Yu Liang, Ya-Hsun Hsueh, and Pei-Chun Lin

**Abstract**—We report on the design and implementation of a simple bio-inspired hexapod driven by a single motor. Aiming for generating the dynamic locomotion of the robot, the design is based on the motion of a spring loaded inverted pendulum (SLIP) and then expanded to the hexapod morphology. The required speed variations and phase offsets of legs are achieved by utilization of non-circular gear pairs in the transmission system. Thus, the robot can be driven by a single DC motor without control effort. The designed alternating tripod gait allows the robot to adequately negotiate with rough terrain as well as to excite dynamic running behavior. The performance of the robot is evaluated experimentally and is quantitatively compared to the SLIP model.

## I. INTRODUCTION

After evolution process, most ground animals are evolved with agile and robust legs, allowing the animals to move elegantly and rapidly over uneven terrain. Thus, research of the legged robots mainly focuses on how to create the maneuverability and to generate animal-like dynamic locomotion. The study of dynamical robotic systems was initiated by the development of monopods in the 80s [1], and following that, various multi-legged robots were developed and reported. For example, the quadruped Scout series [2], quadruped Tekken series [3], hexapod Sprawl series [4, 5], hexapod RHex [6, 7], etc.

Owing to the bio-inspired legged morphology, how to create bio-inspired locomotion in the legged robots is one of the main approaches to perform robot behavioral development. Though geometrical configurations and evolved stages of the animal legs vary significantly, researchers found that through the adequate motion coordination among the legs, animals' dynamic running locomotion in the sagittal plane can be approximated by a simple mathematical model "SLIP" (Spring-Loaded Inverted Pendulum) [8-10], where the body is treated by a point mass and the legs are approximated by a massless spring. As a running "template", SLIP model indeed provides a prescriptive control guidance to the original complex biological or robotic systems which represents empirical "anchors" by sketching the actuation joints and rigid structures [11]. Thus, in the past few decades the successfulness of the dynamic behavior development of the

legged robots is roughly judged by the similarity of the robot's motion characteristics to that of the SLIP model. For example, the hexapod RHex has only one rotational degree of freedom (DOF) per leg, but it can easily generate SLIP-like jogging behavior with its compliant legs. In addition, it also has great ability to negotiate rough terrain owing to the strategy of full-rotation leg reposition. The hexapod iSprawl has carefully tuned leg compliance, and it can be driven by a single motor and generates SLIP-like locomotion.

Inspired by the morphology of RHex with bio-inspired tripod gaits [6] as well as the transmission strategy of iSprawl [4], here we report on the development of a new hexapod robot which has RHex-style configuration and is driven by only one motor. The planar coordinate system in general has three DOFs, and the platform with 2 motion DOFs (i.e., like cars) already has enough mobility to perform planar locomotion. Of course a robot with high active DOFs in certain level is equivalent to high maneuverability and ground adaptiveness. Even though, it is worth to address the feasibility of designing a legged robot to perform versatile behaviors such as walking, running, rough terrain negotiation by simple robotic morphology with minimum number of active DOFs.

The design process started from understanding the dynamic motion of the SLIP model and then expanded its morphology to the hexapod structure because it could deploy the intrinsically stable 2-beat tripod gait for locomotion. In order to create the robust "tripod posture" (i.e., having three legs stand on the ground) at any moment with appropriate stride frequency, worm and worm gear pairs and non-circular gears pair were utilized in the transmission system. In addition, the legs of the robot should act like a spring as the linear spring of the SLIP model. Empirical evaluation revealed that design and fabrication of the ideal linear spring with strong resistance to the lateral force was challenge. In contrast, fabrication of a single-piece material in ring shape with piece cut out was feasible. Thus, the leg with circular shape was adopted in the final robot design, and hereafter the leg is referred to as the "circular leg". And it was evaluated experimentally that the behavior of the robot with dynamical gait indeed fits with the SLIP model.

Section II and Section III describes the design strategy and design of the transmission system, respectively. Section IV discusses the modeling of the circular leg. Section V reports the experiment evaluation, and Section VI concludes the work.

This work is supported by National Science Council (NSC), Taiwan, under contract 100-2628-E-002 -021-MY3.

Authors are with Department of Mechanical Engineering, National Taiwan University (NTU), No.1 Roosevelt Rd. Sec.4, Taipei, Taiwan. (Corresponding email: peichunlin@ntu.edu.tw).

## II. CONSIDERATION AND STRATEGY OF ROBOT DESIGN

Figure 1(a) depicts the SLIP model, which has three system parameters: length of the spring ( $l$ ), stiffness of the spring ( $K$ ), and mass ( $m$ ). A full running stride of the SLIP model can be divided into stance phase and flight phase as shown in Fig. 1(b). The dynamics of the SLIP model in the stance phase can be derived based on the Lagrangian method. As depicted in Fig. 1(a), angle  $\phi$  and the leg length  $l$  are utilized as the generalized coordinates. Cartesian coordinates of the mass in the stance phase,  $(x, y)$ , can be represented as

$$x = l \sin(\phi)$$

$$y = l \cos(\phi). \quad (1)$$

Then, the velocity state can be obtained

$$\begin{aligned} \dot{x} &= l \cos(\phi) \dot{\phi} + \dot{l} \sin(\phi) \\ \dot{y} &= -l \sin(\phi) \dot{\phi} + \dot{l} \cos(\phi) \end{aligned} \quad (2)$$

The kinematic energy  $T$  and potential energy  $V$  of the SLIP model are

$$T = \frac{1}{2} m (\dot{l}^2 + l^2 \dot{\phi}^2) \quad (3)$$

and

$$V = \frac{1}{2} K (l - l_0)^2 + mgl \cos(\phi), \quad (4)$$

respectively. The symbol  $l_0$  and  $g$  represent the natural length of the spring and gravity constant accordingly. Because the ground-contact point is fixed, the ground reacting force doesn't do any work to the system. The energy of system is conservative. By the Lagrangian method

$$\begin{aligned} \frac{d}{dt} \left( \frac{\partial T}{\partial \dot{\phi}} \right) - \frac{\partial T}{\partial \phi} + \frac{\partial V}{\partial \phi} &= 0 \\ \frac{d}{dt} \left( \frac{\partial T}{\partial \dot{l}} \right) - \frac{\partial T}{\partial l} + \frac{\partial V}{\partial l} &= 0, \end{aligned} \quad (5)$$

with energy terms shown in (3) and (4), the following dynamic equations of the SLIP model can be derived

$$\begin{aligned} \ddot{\phi} &= \frac{1}{l} (g \sin(\phi) - 2l \dot{\phi}) \\ \ddot{l} &= l \dot{\phi}^2 - \frac{K}{m} (l - l_0) - g \cos(\phi) \end{aligned} \quad (6)$$

The differential equation of the SLIP model shown in (6) can be expressed in the state-space form

$$\frac{d}{dt} \begin{bmatrix} \phi \\ l \\ \dot{\phi} \\ \dot{l} \end{bmatrix} = \begin{bmatrix} \dot{\phi} \\ \dot{l} \\ (g \sin(\phi) - 2l \dot{\phi})/l \\ l \dot{\phi}^2 - K/m(l - l_0) - g \cos(\phi) \end{bmatrix}, \quad (7)$$

which is utilized for implementation and numerical integration.

Equation (6) and (7) reveals that the leg length is affected by three factors: (i) centrifugal force, (ii) elasticity of leg, and (iii) the gravity. Thus, its period is determined by these three factors. If the variation of angle and its derivative,  $\phi$  and  $\dot{\phi}$ , are both small, the factors (i) and (iii) only affects the equivalent point of the leg. Thus, the period of the leg is determined only by the factor (ii). In addition, the simplified version of the dynamic equations can be represented as

$$\ddot{l} = -\frac{K}{m} (l - l_0), \quad (8)$$

and its solution can be derived as

$$l(t) = c_1 \sin(\sqrt{K}t + \delta) + c_0. \quad (9)$$

This is actually a 1-D hopper, a reduced-order 1-DOF model of the 2-dimensional SLIP.

In the flight phase, the motion is ballistic and affected by gravity only, so the equations of motion can be described as

$$x_f = x_{LO} + \dot{x}_{LO} t$$

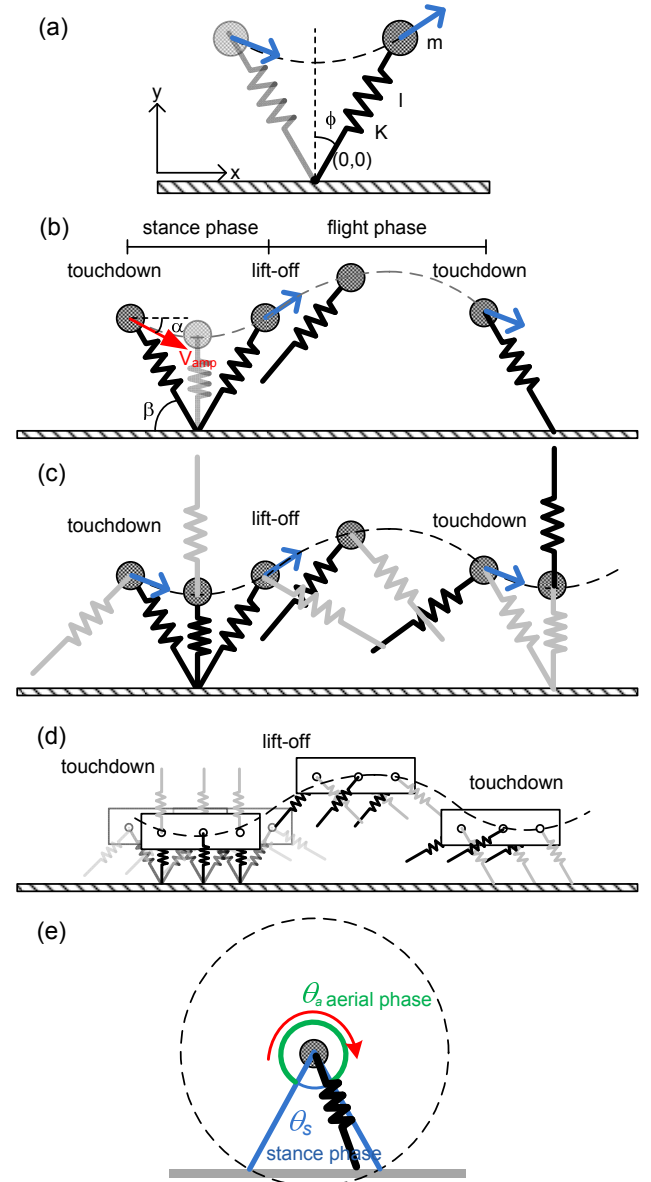


Fig. 1. (a) Intrinsic parameters of the SLIP model. (b)-(d) Motion of various models: (b) trajectory of the SLIP model over a stride; (c) trajectory of running motion with alternating SLIP models; (d) the hexapod robot runs with alternating tripod gait; (e) trajectory of each leg of the hexapod robot.

$$y_f = y_{LO} + \dot{y}_{LO} t - \frac{1}{2} g t^2, \quad (10)$$

where the subscript  $f$  and  $LO$  indicate the flight phase and lift-off, respectively.

The SLIP model shown in (6) and (10) is a conservative system. Thus, the system dynamics in a full stride, including stance and flight phases, can be evaluated with pre-set three system parameters,  $(K, m, l)$ , and chosen initial system conditions. The initial system conditions are usually given at the moment of touchdown (i.e., begin of the stance phase), which includes model landing angle ( $\beta$ ), touchdown speed ( $V_{amp}$ ), and touchdown angle ( $\alpha$ ) included by the touchdown velocity and horizontal line as shown in Fig. 1(b). First, the SLIP model touches the ground. The momentum drives the SLIP moving forward and compressing the spring, which

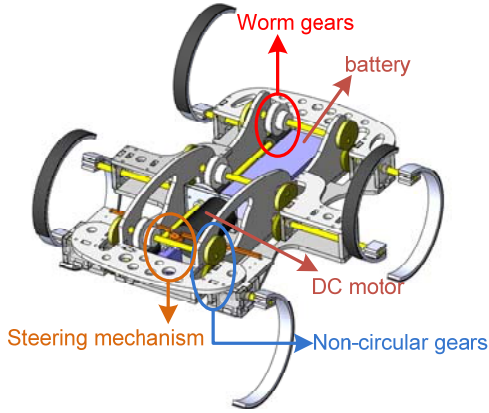


Fig. 2. The 3-dimensional (3D) solid model of the robot, showing the arrangement of the components.

transfers the kinetic energy into elastic potential energy. Next, if the initial touchdown condition is right [9], the spring extends while the mass keeps moving forward, and the SLIP lifts off after the full stretch of the spring. Following that, the SLIP is in the ballistic flight phase, where gravity is the solo external force to the system. After a while, the SLIP touches down the ground again and repeats the motion cycle.

Generally the animals divide the legs into two groups and perform the SLIP-like locomotion alternately as shown in Fig. 1(c) [12]. For example, the human running is executed as a sequence of strides, which alternate between two legs. The insects also run with alternating tripod gait, where three supporting legs in each tripod act as a “virtual spring” for SLIP-like behavior owing to its intrinsic stability, since the center of mass can easily locate in the triangle formed by three supporting legs. Thus, strategy of bio-inspired alternating SLIP-like locomotion is adopted for the robot, and it is served as the “abstract” motion model of the robot.

It is intuitively to coordinate three legs in the same group of the tripod to move in the same manner as shown in Fig. 1(d) since in this strategy: (1) the mapping from three real legs to one virtual leg is straight forward, where the spring constants of the former ones can be summed up and roughly equivalent to that of the latter one; (2) geometrically it is also reasonable to locate the virtual leg right below the COM where the middle real leg locates; (3) in the tripod stance phase, the moments generated from the fore-leg and hind-leg normal to the sagittal plane can be canceled out with each other. If the robot touches down the ground without any pitch angle, it maintains similar configuration at lift-off. This characteristic keeps sagittal-plane motion of the original 6-DOF rigid body robot motion close to the reduce-order SLIP model.

To increase the ground clearance and to enhance the ability of obstacle negotiation, the leg motion in current robot design is periodical rotation in the same direction rather than the animals’ reciprocating motion, like the Buehler Clock in RHex [6]. This setting is shown in Fig. 1(c) and 1(d) in gray springs as well. As shown in Fig. 1(e), the time duration of the stance and aerial phases for each leg are denoted as  $T_s$  and  $T_a$ , respectively, and the rotation angles of the stance and aerial

phases of each leg are denoted as  $\theta_s$  and  $\theta_a$ , accordingly. Thus, the time duration of the robot’s flight phase is  $T_a - T_s$ . Because the time duration of the leg in the aerial phase is roughly about 1 – 1.5 times of that in the stance phase as well as the rotation angles of the leg in the former phase is about 6 times than that in the latter phase, the leg rotating speed in the aerial phase is at least 3-6 times higher than that in the stance phase. This varying rotation speed could be achieved in a simple constant speed driving system by the usage of non-circular gears, since its speed ratio is variable and periodic.

In addition, to generate periodic and continuing locomotion, the phase difference between two tripods has to be fixed at 180 degree, and this phase difference can be created easily by the gear installation with orientation offsets. Based on the above, it is feasible to drive the robot with single motor without position control effort, yet achieving the desired leg trajectories.

About the source of driving system, commercial DC motors usually have high-speed and low-torque output. In contrast, the legged motion is usually operated in the opposite manner, low-speed and high-torque. For example, the stride frequency of animals varies from 1 to 6 Hz. And the larger animals have lower stride frequencies [13]. The Stride frequency of 360g rat jogs is about 1.5-5 Hz, and that of 9200g dog is about 2-4 Hz. For the robot targeting at 3000g, the stride frequency at 3-4Hz is adequate. Thus, a transmission with high speed-reduction characteristics is required between the motor and the non-circular gear pair. In addition, it is desirable to have the robot capable of standing without motor power, which implies the non-backdrivable transmission is preferred. As a result, in addition to the non-circular gear pair, worm and worm gear pair is adopted in the transmission system as well.

Figure 2 depicts the illustrative sketch of the final robot design and component arrangement. The motor power is transmitted through a pair of spur gears to a long shaft installed in the fore-aft direction. The shaft is mounted with three worms, and through the matched worm gears, the motor power is transmitted to the front, middle, and hind shafts mounted in the lateral direction. Between these shafts and the legs, six pairs of the non-circular gears are installed to create the desired speed variation of each legs in one motion cycle as well as to generate the phase difference between two tripods.

Through the model-based design process, the appearance of the final design is indeed similar to RHex [6]. However unlike the 6-DOF RHex which can generate various other kinds of behaviors such as stair climbing [14], pronking [15], bounding, etc. The robot can only perform alternating tripod gaits owing to the trade-off of simple single-motor driving system. Therefore it cannot turn by creating phase difference among legs like RHex, the designed robot is equipped with a steering mechanism on the front legs, to generate car-like turning motion as shown in Fig 2. In short, the novelty and uniqueness of this designed robot lies in its simplicity of two active DOFs with non-controlled motor drive, yet with

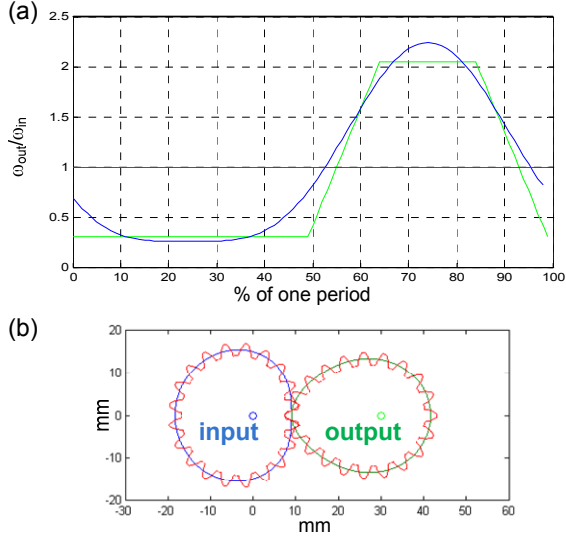


Fig. 3. Design of the non-circular gear pair: (a) the angular velocity profiles of the input gear (red line) and the output gear (original design: green line segments; after smoothing: blue curve); (b) The designed pitch circles (blue curves) and the final gear appearances (red curves).

capability of dynamic ground locomotion and rough terrain negotiation.

### III. DESIGN OF THE NON-CIRCULAR GEAR PAIR

Gear is one kind of transmission which can transfer rotation motion from one shaft to another one. The motion of gear is determined by the “imaginary” rolling circle named pitch circle. For an ordinary spur gear pair, two pitch circles contact and roll with each other all the time. Because of pure rolling, the instant velocity,  $v$ , at interface is the same, for both gears:

$$v = \omega_{in}(\theta)r_{in}(\theta) = \omega_{out}(\theta)r_{out}(\theta), \quad (11)$$

where  $\omega_{in}$  &  $\omega_{out}$  and  $r_{in}$  &  $r_{out}$  are angular velocities and radius of the input and output gears, respectively. The symbol  $\theta$  is the percentage orientation of the input gear in one-turn of rotation (i.e., range from 0 to 1). For non-circular gear pair,  $r$  varies with different  $\theta$ , and because (11) still holds, the  $\omega$  varies accordingly, thus generating variable speed ratio in one turn of gear rotation. Since the distance between shafts,  $s$ , is still fixed

$$r_{in}(\theta) + r_{out}(\theta) = s \quad (12)$$

the radius of the gear can be computed

$$r_{out}(\theta) = s / (1 - \omega_{out}(\theta) / \omega_{in}(\theta)) \quad (13)$$

with given desired speed ratio  $\omega_{out}(\theta) / \omega_{in}(\theta)$ .

With the desired leg rotation profile shown in Fig. 1(e) as the output,  $\omega_{out}$ , and constant-speed rotation from the motor as the input,  $\omega_{in}$ , the speed ratio can be analytically computed.

Figure 3(a) plots the speed ratio of normal gait in one period (i.e., one turn of rotation). Red line indicates the constant-speed rotation of the input gear, which is normalized at one for simplicity. Green line segments depict the pattern of the pre-designed speed profile of the output gear, which is divided into 4 segments: low velocity region, acceleration region, high velocity region, and deceleration region. Since

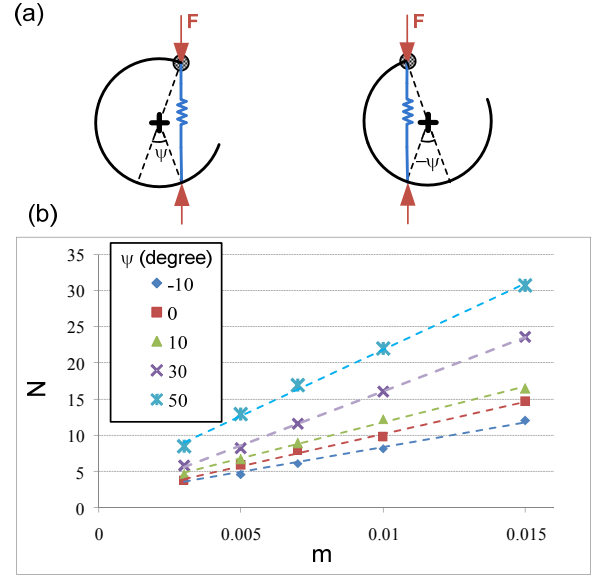


Fig. 4. The evaluation of the stiffness characteristic of the circular leg. Different ground contact points yield different spring constants of 1-DOF reduced-order springs. (a) illustration of the evaluation; (b) empirical measurement.

one-turn to one-turn rotation is designed, the areas under the green and red lines which represent the amount of rotations should be equal. In addition, the area before a half of period roughly equal to  $\theta_s$  shown in Fig. 1(d), representing the leg motion in stance phase. As mentioned before, this angle should be small to maintain the stable tripod gait.

The speed profile of the output gear is further modified to a smooth curve using Fourier series, to reduce the dramatic acceleration and deceleration in transmission:

$$\begin{aligned} \omega_{out}(\theta) &= \frac{1}{2}a_0 + \sum_{n=1}^2 a_n \cos(2\pi n\theta) + b_n \sin(2\pi n\theta) \\ a_n &= 2 \int_0^1 F(t) * \cos(2\pi n\theta) dt \\ b_n &= 2 \int_0^1 F(t) * \sin(2\pi n\theta) dt. \end{aligned} \quad (14)$$

The approximated smooth waveform is shown in blue curve in Fig. 3(a). Because Fourier series would not change the integral in one period, the area below blue curve is the same as that below green line segments. Thus, as long as the pre-design green line segments covers the same area as the blue line does, the constraint of equal rotation angle between input and output non-circular gears is automatically satisfies, even after smoothing.

After adjusting the time ratio of different velocity regions and the low speed ratio to fit wanted gait, the desired speed profile of non-circular gears can be found. Figure 3(b) plots the pitch circles of the designed non-circular gear pair as well as the final teeth based on the involute geometry [16]. The design of single pair is complete.

### IV. DESIGN AND MODELING OF THE CIRCULAR LEG

The desired leg stiffness can be roughly estimated by the locomotion characteristics of the animals. According to [13], the system weighted around 3kg should have stride frequency  $f_s$  in the range of 3 – 4Hz. Because the robot utilizes the alternating tripod gaits, the leg rotation frequency

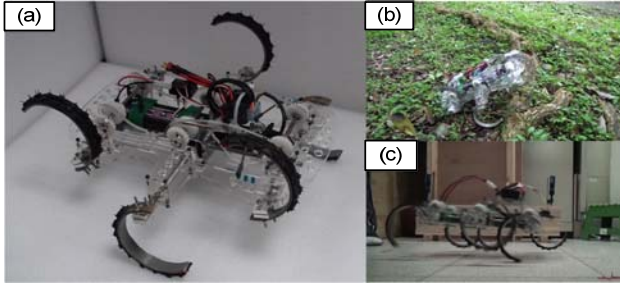


Fig. 5. Photos of the robot: (a) in its standing posture robot; (b) walking on the uneven terrain; (c) performing dynamic behavior with aerial phase.

$f_l$  is half, 1.5 – 2Hz. Next, similar to the approach adopted by the biological research, the 1-DOF spring-mass model is utilized to estimate the leg stiffness [8, 9],

$$f_s = 2f_l = \frac{1}{2\pi} \sqrt{\frac{K}{m}}. \quad (15)$$

In addition, owing to the tripod locomotion, the stiffness (i.e., spring constant) of the real leg should be one-third of  $K$ , and the value is derived to be around 0.75KN/m. Thus number is adopted as the desired spring stiffness of the circular leg.

The circular leg is a complex high-order system, whose motion involves the rolling behavior and change of stiffness. In order to take account of the rolling effect and the change of stiffness, the 1-DOF linear stiffness of the circular leg is empirically measured at various ground-contact points and with different compression force between the hip joint and the ground contact points as shown in Fig. 4(a). The contact points are spanned around  $60^\circ$  around the lower part of the circular leg. Then, the value of the stiffness at the median range is selected as the reduced-order 1-DOF stiffness of the circular leg. Figure 4(b) plots the measured forces versus displacements at these ground-contact points of one of the circular legs under evaluation, and the stiffness are derived to be varied from 0.7KN/m to 1.7KN/m. In this set of measurement, the spring constant 1.1KN/m is chosen as the value which represents the reduced-order 1-DOF stiffness of the circular leg. This value is located at the median range of the original variant spring constants ( $\psi = -30^\circ$  to  $10^\circ$ ).

Theoretically though a lower stiffness value around 0.75KN/m is desired, we found that the empirical circular legs with this stiffness are fragile and easy to break owing to their thin thickness or narrowed width. It cannot survive large deformation induced by dynamic load during robot locomotion. Because the stride frequency of the leg can be operated at a higher value by adequate motor driving, the stiffer circular legs with stiffness 1.1KN/m described in the previous paragraph is adopted for experimental work. According to (15), the new desired stride frequency of the robot with this stiffness value is about 5 Hz. Together with the higher stride frequency, the robot is still operated in the frequency around its natural one. In addition, for performance evaluation, the stiffness 1.1KN/m and the diameter of the circular leg are utilized as the stiffness and length of the ideal SLIP model described in section II.

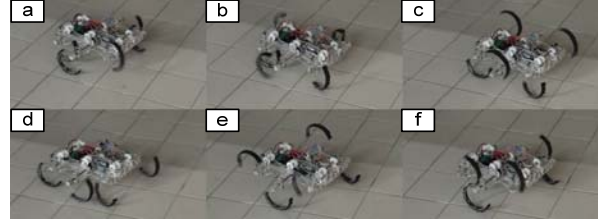


Fig. 6. The sequence pictures of running robot. Robot walks stably and smoothly with tripod gait.

## V. PERFORMANCE EVALUATION

Section II to IV describes various issues of designing a robot which is driven by a single motor and can performance dynamic behaviors. To evaluate the effectiveness of the strategy, a hexapod robot shown in Fig. 5(a) was built for experimental evaluation. Figure 5(b) shows the snapshot of the robot walking outdoor. The legs correctly move according to the designed alternating tripod gait, and consequently, the robot walks stably and smoothly as shown in Figure 6. When the leg stride period decreases, the motion of the robot enters the dynamic region where there exists certain aerial phase as shown in Fig. 5(c). To quantitatively evaluate whether the behavior of the robot matches the mathematical models, a series of robot running tests with different stride frequencies was executed under the ground truth measurement system (GTMS) with the 6-axis force plate on the ground. Thus, body state of the robot and ground reaction force data could be recorded. Because the SLIP is planar, the motion in the sagittal plane was extracted for analysis.

Fig. 7(a) plots the displacement and velocity of the robot in the forward ( $x$ ) and vertical ( $z$ ) directions versus time with stride frequency 6.3Hz. The data is represented in the statistic manner, where the blue curve is the mean of several runs, and standard deviation at several time stamps are also plotted. The trajectory of the SLIP model in Fig. 7(b) computed according to (7) is also plotted for comparison. To compare the models with real robot locomotion more precisely, the initial states of the SLIP model simulation, including touchdown velocity and leg landing angle are roughly extracted from the recorded videos. Figure 7 shows that a moderate match of the body state between the actual robot and the SLIP model. The composition of the robot has certain difference than that of the SLIP model, and we believe the difference is the source of the discrepancy. First, the motion of the circular leg is in some level different than that of the linear spring with fixed stiffness owing to its high-DOF nature. In addition, the ground-contact exhibits slippage. Second, the energy status of the robot and the model is different. The SLIP model is conservative, so its motion relies on the momentum determined by the initial conditions. Thus, if the stride frequency is low, the SLIP may not able to move forward. In contrast, the empirical robot is not energy conservative, which has motor power input to compensate the damping loss. When the robot walks slowly, the power from motor still moves the robot forward. Third, the rolling behavior may

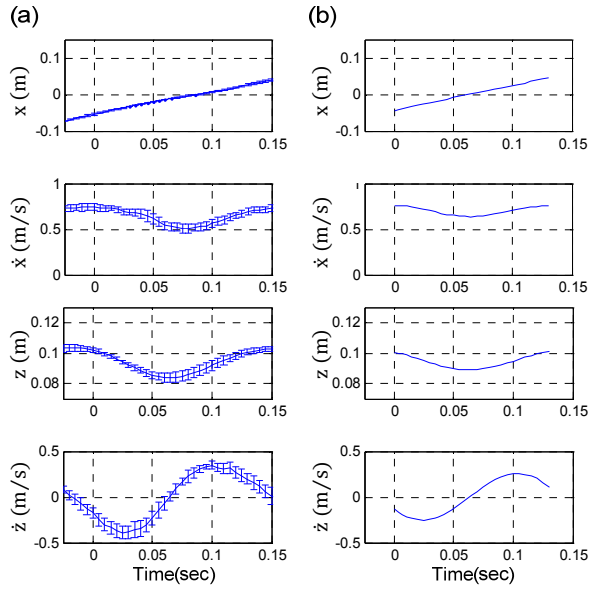


Fig. 7. Comparison of the displacement, velocity (with dot) versus time ( $t$ ) between (a) the experimental robot running data and (b) the SLIP model in the forward direction ( $x$ ) and vertical direction ( $z$ ). The vertical I-shape bars (blue) indicate the standard deviations of the experimental data.

create some discrepancy as well, especially in the forward velocity and the vertical displacement.

Figure 8 plots the ground reaction forces of the robot operated with the stride frequency  $f_s = 6.3$  Hz. The robot indeed exhibits running behavior with flight phase, which can be observed by the vertical ground reaction force data. In addition, the force pattern is close to the measurement of running animals.

## VI. CONCLUSION

We report on the design of a simple bio-inspired hexapod robot with single-motor driving system. The non-circular gear pairs included in the transmission system generates the required speed variation of the leg between its stance phase and flight phase. In addition, with correct phase shift, the alternating tripod motion can be achieved. Thus, the robot can walk stably as the hexapod RHex which has one motor for each leg and is inspiration source of the robot design. The reduce-order 1-DOF model of the compliant circular leg is reported, which guides us to map the locomotion of the robot to the SLIP model. With correct design, the robot can perform SLIP-like locomotion, which is evaluated experimentally and quantitatively.

Currently we are in the process of evaluating the effect of the stride frequency to the overall robot dynamic behavior in detail and to investigate the adequate model with rolling behavior for the circular leg.

## REFERENCES

[1] M. H. Raibert, "Hopping in legged systems - modeling and simulation for the two-dimensional one-legged case," *IEEE Transactions on Systems Man and Cybernetics*, vol. 14, pp. 451-463, 1984.  
 [2] I. Poulakakis, J. A. Smith, and M. Buehler, "Modeling and experiments of untethered quadrupedal running with a bounding gait:

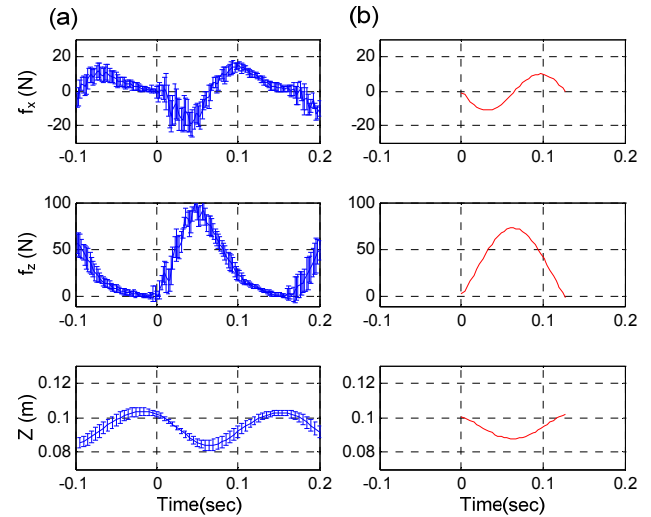


Fig. 8. Comparison of the ground reaction force  $f$  between (a) the experimental robot running data and (b) the SLIP model in the forward direction and in the vertical direction. The vertical COM displacement is plotted below for reference.

The Scout II robot," *International Journal of Robotics Research*, vol. 24, pp. 239-256, Apr 2005.  
 [3] H. Kimura, Y. Fukuoka, and A. H. Cohen, "Adaptive dynamic walking of a quadruped robot on natural ground based on biological concepts," *International Journal of Robotics Research*, vol. 26, pp. 475-490, May 2007.  
 [4] S. Kim, J. E. Clark, and M. R. Cutkosky, "iSprawl: Design and tuning for high-speed autonomous open-loop running," *International Journal of Robotics Research*, vol. 25, pp. 903-912, Sep 2006.  
 [5] J. G. Cham, J. K. Karpick, and M. R. Cutkosky, "Stride period adaptation of a biomimetic running hexapod," *International Journal of Robotics Research*, vol. 23, pp. 141-153, Feb 2004.  
 [6] U. Saranli, M. Buehler, and D. E. Koditschek, "RHex: A simple and highly mobile hexapod robot," *International Journal of Robotics Research*, vol. 20, pp. 616-631, Jul 2001.  
 [7] P. C. Lin, H. Komsuoglu, and D. E. Koditschek, "Sensor data fusion for body state estimation in a hexapod robot with dynamical gaits," *IEEE Transactions on Robotics*, vol. 22, pp. 932-943, Oct 2006.  
 [8] R. Blickhan, "The spring mass model for running and hopping," *Journal of Biomechanics*, vol. 22, pp. 1217-1227, 1989.  
 [9] P. Holmes, R. J. Full, D. Koditschek, and J. Guckenheimer, "The dynamics of legged locomotion: Models, analyses, and challenges," *Siam Review*, vol. 48, pp. 207-304, Jun 2006.  
 [10] R. M. Alexander, *Elastic mechanisms in animal movement* Cambridge University Press 1988.  
 [11] R. J. Full and D. E. Koditschek, "Templates and anchors: Neuromechanical hypotheses of legged locomotion on land," *Journal of Experimental Biology*, vol. 202, pp. 3325-3332, Dec 1999.  
 [12] J. Seipel and P. Holmes, "A simple model for clock-actuated legged locomotion," *Regular & Chaotic Dynamics*, vol. 12, pp. 502-520, Oct 2007.  
 [13] N. C. Heglund, C. R. Taylor, and T. A. McMahon, "Scaling stride frequency and gait to animal size: mice to horses," *Science*, vol. 186, pp. 1112-3, 1974.  
 [14] E. Z. Moore, D. Campbell, F. Grimmering, and M. Buehler, "Reliable stair climbing in the simple hexapod RHex," in *International Conference on Robotics and Automation*, 2002, pp. 2222-2227.  
 [15] D. McMordie and M. Buehler, "Towards pronking with a hexapod robot," in *International Conference on Climbing and Walking Robots and the Support Technologies for Mobile Machines* 2001, pp. 659-666.  
 [16] F. L. Litvin, A. Fuentes-Aznar, I. Gonzalez-Perez, and K. Hayasaka, *Noncircular gears: Design and generation* Cambridge University Press 2009.